Molecular-Level Simulations of Shock Generation and Propagation in Soda-Lime Glass

M. Grujicic, W.C. Bell, B. Pandurangan, B.A. Cheeseman, C. Fountzoulas, and P. Patel

A non-equilibrium molecular dynamics method is employed to study the mechanical response of soda-lime glass (a material commonly used in transparent armor applications) when subjected to the loading conditions associated with the generation and propagation of planar shock waves. Specific attention is given to the identification and characterization of various (inelastic-deformation and energy-dissipation) molecular-level phenomena and processes taking place at, or in the vicinity of, the shock front. The results obtained revealed that the shock loading causes a 2-4% (shock strength-dependent) density increase. In addition, an increase in the average coordination number of the silicon atoms is observed along with the creation of smaller Si-O rings. These processes are associated with substantial energy absorption and dissipation and are believed to greatly influence the blast/ballistic impact mitigation potential of soda-lime glass. The present work was also aimed at the determination of the shock Hugoniot (i.e., a set of axial stress vs. density/specific-volume vs. internal energy vs. particle velocity vs. temperature) material states obtained in soda-lime glass after the passage of a shock wave of a given strength (as quantified by the shock speed). The availability of a shock Hugoniot is critical for construction of a high deformation-rate, large-strain, high pressure material model which can be used within a continuum-level computational analysis to capture the response of a soda-lime glass based laminated transparent armor structure (e.g., a military vehicle windshield, door window, etc.) to blast/ballistic impact loading.

1. Introduction

Transparent blast/ballistic-impact resistant vehicle structures (e.g., windshields, door windows, viewports, etc.), employed today, utilize a variety of non-glass transparent materials such as transparent crystalline ceramics (e.g., aluminum-oxinitride spinel, AlON, sapphire (Ref 1) and new transparent polymer materials (e.g., transparent nylon (Ref 2)). Despite the well-established benefits offered by these materials, ballistic glass remains an important constituent material in a majority of transparent impact resistant structures used today. The main reason for this are as follows: (a) glass-structure fabrication technologies enable the production of curved, large surface-area, transparent structures with thickness approaching several inches; (b) relatively low material and manufacturing costs; and (c) compositional modifications, chemical strengthening, and controlled crystallization have demonstrated the capability to significantly improve the shock/ballistic impact survivability of glass (Ref 2).

Typically, the development of new glass-based transparent impact resistant structures, aimed at reducing the vulnerability of protected vehicle occupants and on-board instrumentation to various blast/ballistic threats, requires extensive prototyping and laboratory/field experimental testing. These experimental efforts are critical for ensuring the effectiveness and reliability of the transparent impact resistant structures.

However, these efforts are generally expensive, time-consuming, and involve destructive test procedures. While the role of prototyping/testing programs remains critical, they are increasingly being complemented by the corresponding computation-based modeling and simulation efforts. It is well-established (Ref 3–5), that the effectiveness and reliability of the computation-based modeling and simulation approaches is greatly affected by the fidelity of the associated material models. It is critical that these models realistically describe deformation/fracture response of the subject material (ballistic glass, in the present case) under high-rate, large-strain, high-pressure loading conditions encountered during blast/ballistic impact. Therefore, one of the main objectives of the present work is to further advance the application of computational modeling/simulation-based engineering approaches of transparent impact-resistant structures via the identification and quantification of processes and phenomena occurring in glass under such conditions. Specifically, phenomena and processes associated with the formation and propagation of shock waves within soda-lime glass will be investigated.

A comprehensive literature review carried out as part of our prior work (Ref 6) revealed that the mechanical behavior of glass is modeled predominantly using three distinct approaches: (a) molecular-modeling methods (Ref 7–10); (b) continuum-material approximations (Ref 3–5, 11–14); and (c) models based on explicit crack representation (Ref 15, 16). Since a

M. Grujicic, W.C. Bell, and **B. Pandurangan**, Department of Mechanical Engineering, Clemson University, 241 Engineering Innovation Building, Clemson, SC 29634-0921; and **B.A. Cheeseman, C. Fountzoulas,** and **P. Patel**, Army Research Laboratory – Survivability Materials Branch, Aberdeen, Proving Ground, MD 21005-5069. Contact e-mails: gmica@exchange.clemson.edu and gmica@clemson.edu.

detailed overview of these models can be found in Ref 6, they will not be discussed any further in the present manuscript. However, what is worth mentioning is that the overview presented in Ref 6 clearly established that: (a) molecular-level models are critical for identifying nanometer length scale phenomena and the associated microstructure evolution processes; (b) continuum-level models are the only ones which enable large-scale computational analysis of the mechanical response of real transparent-armor protective structures to various blast and ballistic threats; and (c) the models based on explicit crack propagation are mainly suitable for modeling local deformation and fracture response of simple-geometry test coupons. Since the main objective of the present work is to help identify and characterize various phenomena and processes accompanying shock generation and propagation within soda-lime glass, only the molecular-level computational models and methods will be employed.

As mentioned above, the main objective of the present work is to investigate various shock wave-related phenomena using molecular-level computational methods.

A shock wave (or simply a shock) is a wave which propagates through a medium at a speed higher than the sound speed and its passage causes an abrupt and discontinuous change in the material state variables (e.g., pressure, internal energy, density, temperature, and particle velocity). The magnitude of the state-variable changes and the shock speed increase with the strength of the shock. While acoustic waves give rise to isentropic changes in the material state variables, passage of a shock is typically associated with irreversible (entropy-increasing) changes in the same variables. The reason behind this difference is that shock involves very high strain rates that bring energy-dissipative viscous effects into prominence.

A review of the literature carried out as a part of the present work revealed that the molecular-level computational methods were first employed to study shock waves more than 30 years ago (Ref 17–20). While the initial studies focused on shock phenomena in dense fluids, subsequent work also included single-crystalline solids. The key findings related to the generation and propagation of shocks in these solids can be summarized as follows: (a) these phenomena are inherently more complex in solids than in fluids, because solids, in addition to the lattice parameter, introduce a new length scale (i.e., the size/spacing of defects) which tends to control the nature/extent of inelastic-deformation and dissipative processes at the shock front; (b) shock propagation typically results in the formation of steady (time-invariant) waves, and this process is facilitated by the transverse displacement of atoms which produce inelastic deformation. This deformation involves concerted slippage of atoms over each other (and not viscous flow as in the case of shocks in fluids); (c) in order to eliminate free-surface effects, molecular-level modeling of shock is typically carried out using computational systems with periodic boundary conditions (at least in directions transverse to the shock-wave propagation direction). To attain steady wave conditions of the shock, computational domains sufficiently long in the direction of shock-wave propagation have to be employed. Furthermore, lateral dimensions of the computational domain have to be also sufficiently large to avoid spurious effects associated with the use of the periodic boundary conditions. Consequently, computational domains involving several tens to hundred thousands of atoms have to be employed. The corresponding computational times (con-trolled by the shock-wave transversal time) are then on the order of 5-20 ps. This limits the shock thicknesses to around 10 nm and the corresponding rise times to ca. 0.5-1 ps. Thus, weak shock waves with thicknesses of hundreds of nanometers could not be analyzed using molecular-level methods (at least in their steady-wave regime).

While recognizing the aforementioned aspects and potential limitations of molecular-level modeling of shock, a preliminary computational study of shock generation/propagation in soda-lime glass is carried out. There are two main objectives of the present work:

(a) To determine the shock Hugoniot (centered on the initial stress-free quiescent state) of soda-lime glass. A Hugoni-ot is the locus of axial stress vs. specific volume vs. energy density (vs. particle velocity vs. shock speed) shocked ("upstream") material states. The Hugoniot is often used in the derivation of the continuum-level material models (particularly in the derivation of the equation of state) which is used in the computational investigations of the response of structures to shock loading. In situations in which one is interested only in the problem of planar shock propagation/interaction (in the presence of uni-axial strain deformation states), a complete definition of the continuum-level material model is not required. Instead, the knowledge of the corresponding Hugoniot relations is sufficient; and

(b) The Hugoniot relations mentioned in (a) provide a global statement of mass, momentum, and energy conservation accompanying shock-induced material transition from a given initial ("downstream") equilibrium state to all possible final ("upstream") equilibrium states for steady planar shock waves (of different strengths). However, these relations provide no information about the structure of the shock front or the nature of the dissipative structural rearrangement mechanisms that lead to a steady shock wave. Hence, the second objective of the present work is to carry out a detailed examination of the downstream, shock-front, and upstream material states (as represented by the local stresses, strains, densities/specific volumes, temperatures, etc.) and molecular-level morphology to identify and characterize these processes.

The organization of the paper is as follows: A brief description of the molecular-level microstructure of glass including its random-network representation is presented in Sect. 2. A brief overview of the molecular-level computational procedure including the computational cell construction, force field identification, computational method(s) selection, shock-wave generation, and the problem definition are, respectively, presented in Sects. 3.1-3.5. The key results obtained in the present work are presented and discussed in Sect. 4. A summary of the work carried out and the key results/conclusions are given in Sect. 5.

2. Molecular-Level Microstructure of Glass

One of the basic properties of all types of glass is their lack of long-range atomic order which classifies them as amorphous materials. For instance, the atomic arrangement in pure silicate

glass (i.e., fused silica) is highly random relative to the chemically equivalent (crystalline) quartz. To describe the random atomic arrangement within glass the so-called "random network model" (Ref 21) is typically employed. Such a model represents amorphous materials as a three-dimensional linked network of polyhedra with central cations of various coordination depending on the character of the atomic constituents. In the case of silicate-based glasses like fused silica and soda-lime glass, the dominant cation is silicon. In this case, each silicon is surrounded by four oxygen anions and forms a SiO_4^{4-} tetrahedron, whereby each oxygen is bonded to (or bridges) two silicon atoms. Other polyhedra may exist in the network depending on the glass additives. Since silicon has a tendency to form a continuous network with (bridging) oxygen atoms, SiO_2 is commonly referred to as a "network former". Other potential network formers in glass are boron and germanium oxides.

Numerous oxides and other additives are used to modify the basic silica tetrahedra network of silicate-based glasses to tailor their properties to specific applications. When alkali (or alkaline earth) oxides are added to a pure silicate-based glass, in order to accommodate the excess of oxygen anions which are present due to the oxide dissociation, the continuity of the silica tetrahedra network becomes disrupted. The resulting glass structure contains additional non-bridging (connected to only one silicon atom) oxygen atoms. Charge transfer from the alkali earth metal atoms converts the non-bridging oxygen atoms into singly charged anions. The metallic cations formed in this process tend to hover around the non-bridging oxygen ions for local charge neutrality. Since alkali (or alkaline earth)-based oxides cause a disruption in the continuous glass network, they are typically referred to as "network modifiers". In the specific case of soda-lime glass, the 14 wt.%Na_2O and 9 wt.%CaO additions to the silica both act as network modifiers.

In contrast to network modifying oxides, more covalently bonded oxides like B_2O_3 donate metallic cations which become incorporated into the glass network without significant compromise in the network connectivity. In other words, the addition of these oxides does not lead to the formation of non-bridging oxygen atoms. Due to the aforementioned behavior of these glass-oxides additives they are typically referred to as network formers.

For the purpose of quantitative description of the microstructure within the random network model, a number of network parameters have been introduced. For instance, a so-called R value (defined as the average number of oxygen ions per network forming ion) is used to describe the overall connectivity of a given network. In the case of fused silica, in which there are two (bridging) oxygen anions for every network forming silicon cation, the R value is 2.0. In the case of soda-lime glass, the introduction of non-bridging oxygen ions causes the R value to increase to ca. 2.41. This finding suggests that a higher R value is associated with a more open (less connected) weaker amorphous glass network. As far as the network formers are concerned their effects on the glass microstructure and the R value is greatly affected by the cation coordination number and the strength of its bond with oxygen as well as to the concentration of the additive. In addition to the R value, the so-called "X" and "Y" parameters are often used to further quantify the glass network structure. These two parameters are, respectively, defined as the average number of non-bridging (connected to only a single network forming cation) and bridging (connected to two network forming cations) oxygen atoms per network polyhedron. Since pure silicate-based glasses contain only bridging oxygen atoms (and are based on silica tetrahedra), the X and Y parameters take on values of 0.0 and 4.0, respectively. On the other hand, since soda-lime glass contains additional non-bridging oxygen atoms (while its network is still based on silica tetrahedral), X takes on a non-zero value (ca. 0.81) while Y drops below 4.0 (ca. 3.19).

In addition to chemical modifications of glass, changes in the microstructure of this material can be brought about by mechanical loading/deformation (typically requiring several GPa pressure levels). Specifically, high pressure may result in a reorganization of the atomic network (phase change) in the form of changes to the coordination of the network forming cations. These phase changes can be of first order, which are characterized by the formation a distinct high-pressure phase at a nominally constant pressure, or they may be of second order which are phase changes which involve a continuous morphing of the original phase into the final high-pressure phase over a range of pressures. These phase transformations may be associated with significant volume changes and, since phase-transformation induced energy absorption is a well-documented phenomenon responsible for high toughness levels in TRIP steels and partially stabilized crystalline ceramics, it is of interest to the present study.

The phase transformations of glass which are investigated in the present work occur in the range of 3 to 5 GPa and are thought to be of first order. This pressure range was chosen for the current investigation as it is consistent with the levels seen in glass structures subject to ballistic/blast loading and is associated with relatively modest (3-7%) volume changes. These phase transformations should not be confused with those seen to take place at substantially higher pressures (ca. >20 GPa), which are considered to be of second order and associated with substantially larger volume reductions and with the formation of stishovite, an octahedrally coordinated glass phase.

3. Molecular-Level Analysis of Soda-Lime Glass

As mentioned earlier, molecular-level computational methods have been employed in the present work to investigate shock formation and propagation in soda-lime glass. Within these methods, all atoms, ions and bonds are explicitly accounted for and molecular mechanics, dynamics or Monte Carlo algorithms are used to quantify the behavior of the material under investigation.

While ab initio quantum mechanics methods have the advantage over the molecular-level methods since they do not require parameterization, they have a serious short-coming. Namely, due to prohibitively high computational cost, they can be currently employed only for systems containing no more than a few hundred atoms/particles. As will be shown below, while ab initio quantum-mechanics calculations are not directly used in the present work, some of the computational ab initio quantum mechanics results are used in the parameterization of the material model at the molecular length/time scale. Utility of the molecular-level computational results is greatly dependent on accuracy and fidelity of the employed force field (the mathematical expression which describe various bonding and non-bonding interaction forces between the constituents of the molecular-level model). In the present work, the so-called

"Condensed-phase Optimized Molecular Potentials for Atomistic Simulation Studies" (COMPASS) force field is used (Ref 22, 23). This highly accurate force field is of an ab initio type since most of its parameters were determined by matching the predictions made by the ab initio quantum mechanics calculations to the condensed-matter experimental data. Hence, it should be recognized that the COMPASS force field is a prime example of how the highly accurate results obtained on one length/time scale (quantum mechanic/electronic, in the present case) and the experimental data can be combined to parameterize material models used at coarser length/time scale (the molecular length/time scale, in the present case).

Formulation of a molecular-level simulation problem requires, at a minimum, specification of the following three aspects: (a) a molecular-level computational model consisting of atoms, ions, functional groups, and/or molecules; (b) a set of force field functions; and (c) a computational method(s) to be used in the simulation. More details of these three aspects of the molecular-level modeling and simulation of soda-lime glass are provided below.

3.1 Computational Model

At the molecular level, soda-lime glass is modeled as a discrete material consisting of: (a) silicon (Si) and oxygen (O) atoms mutually bonded via a single covalent bond and forming a connected, non-structured/amorphous network of silica (SiO_4^{4-}) tetrahedra; (b) oxygen anions (O^{2-}) attached as terminal functional groups to the fragmented silica tetrahedra network; and (c) sodium cations (Na^+) dispersed between fragmented silica tetrahedra networks and ionically bonded to the oxygen anions.

While glass is an amorphous material and does not possess any long-range regularity in its atomic/molecular structure, modeling of bulk behavior of glass is typically done at the molecular level by assuming the existence of a larger (amorphous) unit cell. Repetition of this cell in the three orthogonal directions (the process also known as application of the "periodic boundary conditions") results in the formation of an infinitely large bulk-type material. This procedure was adopted in the present work.

The parallelopiped-shaped computational cell used in the present work contained 2304 particles (Si-512, Na^+-512, O^--256 and O-1024). The computational cell edge-lengths were initially set to $a = 7.471$ nm and $b = c = 1.868$ nm, yielding a soda-lime glass initial nominal density of 2.613 g/cm^3. The three edges (a, b, and c) of the cell were aligned, respectively, with the three coordinate axes (x, y, and z).

To create the initial particle configuration in the unit cell, the Visualizer (Ref 24) program from Accelrys was first used to construct a short silica-chain fragment. The fragment was then "grown" by a duplicate-and-attach process using the same program. The resulting silica network (along with additional sodium cations and oxygen anions) was next used within the Amorphous Cell program (Ref 25) from Accelrys to randomly populate the computational cell while ensuring that the target material density of 2.613 g/cm^3 was attained. An example of a typical molecular-level topology within a single unit cell is displayed in Fig. 1.

3.2 Force Fields

As stated above, the behavior of a material system at the molecular-level is governed by the appropriate force fields
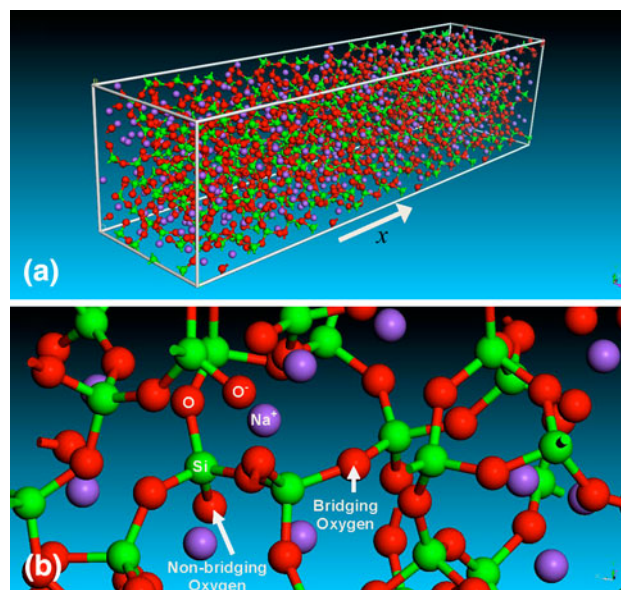

Fig. 1 (a) The computational unit cell for soda-lime glass molecular-level simulations used in the present work; and (b) an example of the local atomic structure

which describe, in an approximate manner, the potential energy hyper-surface on which the atomic nuclei move. In other words, the knowledge of force fields enables determination of the potential energy of a system in a given configuration. In general, the potential energy of a system of interacting particles can be expressed as a sum of the valence (or bond), $E_{valence}$, cross-term, $E_{cross-term}$, and non-bond, $E_{non-bond}$, interaction energies as:

$$E_{total} = E_{valence} + E_{cross-term} + E_{non-bond} \qquad (Eq\ 1)$$

The valence energy generally includes a bond stretching term, E_{bond}, a two-bond angle term, E_{angle}, a dihedral bond-torsion term, $E_{torsion}$, an inversion (or an out-of-plane interaction) term, E_{oop}, and a Urey-Bradlay term (involves interactions between two atoms bonded to a common atom), E_{UB}, as

$$E_{valence} = E_{bond} + E_{angle} + E_{torsion} + E_{oop} + E_{UB} \qquad (Eq\ 2)$$

The cross-term interacting energy, $E_{cross-term}$, accounts for the effects such as bond length and angle changes caused by the surrounding atoms and generally includes: stretch-stretch interactions between two adjacent bonds, $E_{bond-bond}$, stretch-bend interactions between a two-bond angle and one of its bonds, $E_{bond-angle}$, bend-bend interactions between two valence angles associated with a common vertex atom, $E_{angle-angle}$, stretch-torsion interactions between a dihedral angle and one of its end bonds, $E_{end\_bond-torsion}$, stretch-torsion interactions between a dihedral angle and its middle bond, $E_{middle\_bond-torsion}$, bend-torsion interactions between a dihedral angle and one of its valence angles, $E_{angle-torsion}$, and bend-bend-torsion interactions between a dihedral angle and its two valence angles, $E_{angle-angle-torsion}$, terms as:

$$
\begin{aligned}
E_{cross-term} =& E_{bond-bond} + E_{angle-angle} + E_{bond-angle} \\
&+ E_{end\_bond-torsion} + E_{middle\_bond-torsion} \\
&+ E_{angle-torsion} + E_{angle-angle-torsion} \qquad (Eq\ 3)
\end{aligned}
$$

The non-bond interaction term, $E_{non-bond}$, accounts for the interactions between non-bonded atoms and includes the van

der Waals energy, E_{vdW}, and the Coulomb electrostatic energy, $E_{Coulomb}$, as:

$$E_{non\text{-}bond} = E_{vdW} + E_{Coulomb} \qquad (Eq\ 4)$$

As mentioned earlier, the present molecular-level analysis of soda-lime glass employs the COMPASS (Ref 22, 23) force field for various bond and non-bond interaction energies appearing in Eqs 1-4. A summary of the COMPASS force-field functions can be found in our previous work (Ref 26).

3.3 Computational Method

Both molecular statics and molecular dynamics simulations were employed in the present work. Within the molecular statics approach, the unit-cell potential energy (as defined by Eqs 1-4) is minimized with respect to the position of the constituent particles/atoms. The potential energy minimization within Discover (Ref 27) (the atomic simulation program from Accelrys used in the present work) is carried out by combining the Steepest Descent, Conjugate Gradient, and the Newton's minimization algorithms. These algorithms are automatically inactivated/activated as the atomic configuration is approaching its energy minimum (i.e., the Steepest Descent method is activated at the beginning of the energy minimization procedure while the Newton's method is utilized in the final stages of this procedure).

As will be discussed in greater detail in Sect. 4, molecular statics is employed to determine the state of the material swept by a shock. As will be shown, this procedure is based on the use of (bonding and non-bonding) potential energy components and neglects shock-induced changes in the (configurational) entropy of the system. To assess the consequence of this simplification, the approach described in Ref 28 was considered. This approach defines a dimensionless parameter and states that when this parameter is significantly smaller than unity, entropy effects can be neglected. Unfortunately, detailed temperature and pressure dependencies of the material mechanical response of soda-lime glass needed to evaluate this parameter were not available with sufficient fidelity. Hence, the results obtained by the application of this procedure, which suggest that the entropy effects may not be highly critical, cannot be accepted with a high level of confidence.

Within the molecular dynamics approach, gradient of the potential energy with respect to the particle positions is first used to generate forces acting on the particles and, then, the associated Newton's equations of motion (for all particles) are integrated numerically to track the temporal evolution of the particle positions. Both the equilibrium and non-equilibrium molecular dynamics methods are employed in the present work. Within the equilibrium molecular-dynamics methods, the system under consideration is coupled to an (external) environment (e.g., constant pressure piston, constant temperature reservoir, etc.) which ensures that the system remains in equilibrium (i.e., the system is not subjected to any thermodynamic fluxes). As will be discussed in next section, NVT (where N is the (fixed) number of atoms, V, the computational cell volume (also fixed), and T (298 K) is the temperature) equilibrium molecular dynamics is employed in the first stage of the shock generation procedure. In addition, as will be discussed in Sect. 4, NVE (E is the total energy) equilibrium molecular dynamics is also employed during determination of the shock Hugoniot. Within non-equilibrium molecular dynamics, the system is subjected to large perturbations (finite

changes in the axial parameter of the computational cell, in the present case) which create a thermodynamic flux (i.e., the flux of energy and momentum, in the present case). More details regarding the use of Discover to carry out molecular statics and molecular dynamics analyses can be found in our prior work (Ref 6).

3.4 Shock-Wave Generation

To generate a planar shock (or more precisely a pair of planar shocks) within the computational cell, the following procedure is employed:

(a) At the beginning of the analysis, a "sufficiently long" NVT molecular dynamics simulation is carried out to equilibrate the system/material.
(b) The shock is then initiated (and driven) by continuously contracting the computational cell x-direction lattice parameter a as:

$$a(t) = a(t = 0) - 2u_p t \qquad (Eq\ 5)$$

where t denotes time, u_p is the so-called "piston" velocity (or equivalently the particles upstream velocity) in the x-direction. u_p is varied over a range between 187.5 and 1500 m/s to simulate the generation and propagation of shock of various strengths. Meanwhile, computational-cell transverse lattice parameters b and c are kept constant to obtain planar (uniaxial-strain) shock conditions. In this process, the computational cell faces normal to the shock propagation-direction behave very similarly to the impact surface of a plate-like target subjected to a so-called symmetric "flyer-plate" impact test (Ref 29). The procedure employed here generates a pair of shock waves which propagate, at a shock speed U_s, from the cell boundaries toward its center. As schematically shown in Fig. 2, these shock waves leave behind a "shocked" material state characterized by a higher material density (as well as internal energy, temperature, stress, particle velocity, and entropy).
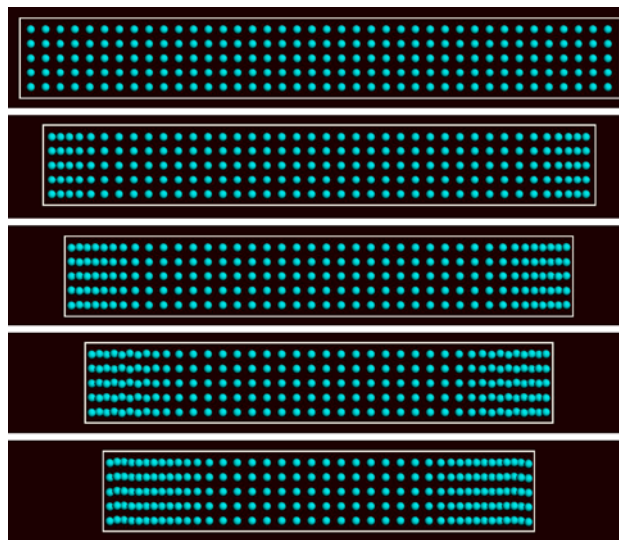

Fig. 2 A schematic of the generation of a pair of shocks in a molecular-level system via the process of computational-cell parameter contraction

The aforementioned procedure for shock-wave generation and the subsequent molecular statics/dynamics analyses are carried out through the use of a Discover input file (Ref 27) which is written in a Basic Tool Command Language (BTCL). This enabled the use of a scripting engine that provides very precise control of simulation jobs, e.g., a cell deformation to be carried out in small steps each followed by a combined energy-minimization/molecular-dynamics simulation run.

3.5 Problem Formulation

The problem addressed in the present work involved generation of shock waves of different strengths (using the aforementioned computational cell parameter contraction method), determination of the associated shock Hugoniot relations and identification and elucidation of the main molecular-level inelastic-deformation/energy dissipation processes taking place at or in the vicinity of the shock front. The procedure for shock-wave generation was presented in the previous section.

As far as the shock Hugoniot determination is concerned, it entailed the knowledge of the shock-wave profiles (and their temporal evolution) for the axial stress, material density, particle velocity, internal energy, and temperature. The latter are obtained by lumping particles/atoms and their (bond and non-bond) potential and kinetic energy contribution, into fixed-width bins, in the order of their axial coordinates. As will be shown in the next section, two types of bins are used: (a) a Lagrangian-type which is fixed to the initial/reference state of the computational cell and (b) a moving-type which is attached to the advancing shock front.

Identification of the molecular-level inelastic-deformation/energy dissipation processes entailed a close examination of the changes in a material bond structure and topology caused by the passage of the shock.

4. Results and Discussion

4.1 Shock-Wave Observation and Structure Characterization

An example of the typical results, obtained in the present work, pertaining to material molecular-level microstructure/topology evolution caused by a continuous axial contraction of the computational cell is displayed in Fig. 3(a)-(d). The results displayed in this figure clearly reveal the generation of a pair of planar shock waves at the two opposing y-z faces of the computational cell, Fig. 3(a), and their subsequent propagation toward the center of the cell, Fig. 3(b)-(d). An approximate location of the center point of the two shocks is indicated using arrowheads in Fig. 3(a)-(d). The results displayed in Fig. 3(a)-(d) show that the shock waves remain fairly planar during their motion. While the two shocks collide at a later simulation time, a shock-wave interaction investigation is beyond the scope of the present work.

While the results displayed in Fig. 3(a)-(d) provide clear evidence for the formation and propagation of a pair of opposing planar shock waves, they do not offer any information about the structure/shape of the shock-wave front or about the state of the (upstream) material swept by the shock. The latter aspects of shock-wave generation and propagation within soda-lime glass are addressed in the remainder of this section and in the subsequent sections.
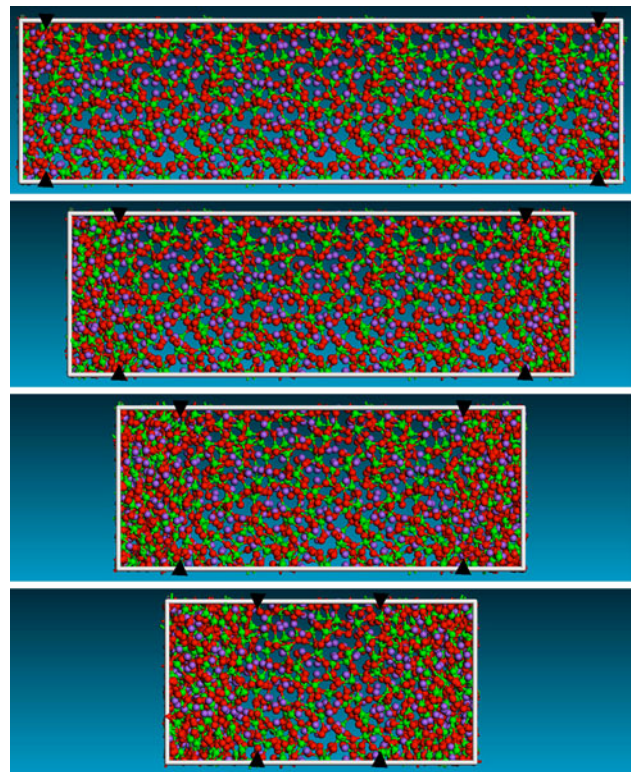

Fig. 3 Temporal evolution of the molecular level material microstructure accompanying generation and propagation of a pair of planar shocks in soda-lime glass

To reveal the structure/shape of the shock wave, the method of (Lagrangian) bins described in Sect. 3.4 is employed. In this case, the bins are fixed in the (initial) reference configuration of the computational cell. In other words, the same atoms are associated with a given bin throughout the entire molecular dynamics simulation. Examples of the typical results obtained through the use of this method are displayed in Fig. 4(a)-(b). The results displayed in this figure are obtained under identical conditions except for the rate of axial contraction of the computational cell (100% higher in the case of Fig. 4(b)). In these figures, particle velocities at different simulation (i.e., post-shock wave generation) times are plotted against the Lagrangian bin center x-location (for the shock propagating to the right, only). Brief examination of the results displayed in Fig. 4(a)-(b) reveals that:

(a) two shock waves are generated (only the right-propagating shock is shown though) at the computational cell faces normal to the x-direction. These shocks subsequently propagate towards the computational-cell center;

(b) after a brief transient period, the shocks appear to attain steady wave profiles (i.e., a time-invariant profile within a reference frame which is attached to, and moves with, the shock front); and

(c) both the particle velocity and the shock speed increase with the computational-cell contraction rate. It should be noted that the curves bearing the same numerical label in Fig. 4(a)-(b) correspond to the same simulation time.

It should also be noted that no thermostat was used in the present non-equilibrium molecular dynamics simulations, so
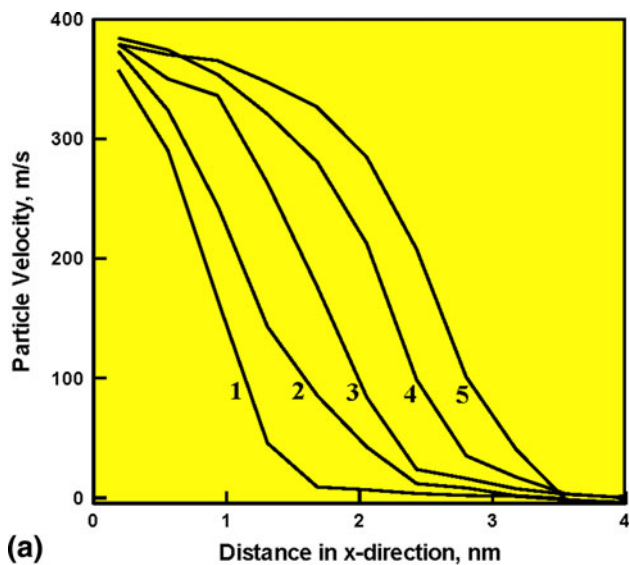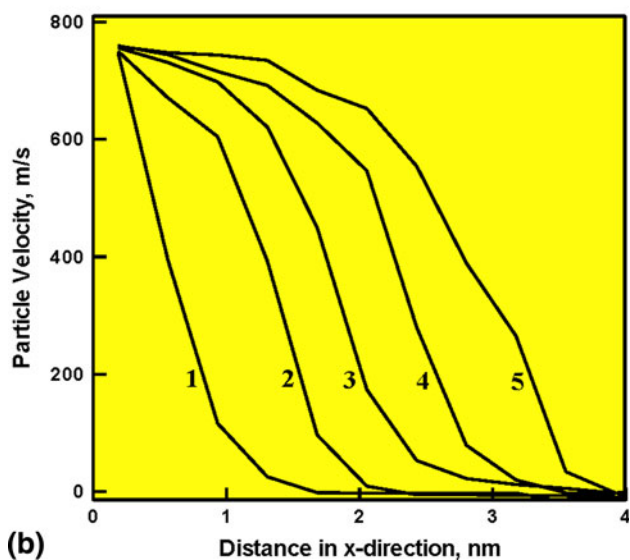
Fig. 4 Temporal evolution of the particle velocity associated with the propagation of two approaching shock waves. The results in (b) are associated with a 50% higher computational-cell axial contraction rate

Fig. 5 The Hugoniot relation pertaining to the particle velocity dependence of the shock speed

that the steady-wave shock profile is a natural consequence of a balance between the continuous supply of momentum to the system (through the continuous computational cell axial contraction) and the observed lateral motion of the atoms in the continuously enlarged upstream material domain swept by the shock. In general, the use of a thermostat modifies the ($F = ma$ Newtonian-type) equations of motion solved within the molecular dynamics simulations by the introduction of a (velocity-proportional) viscous-dissipation term. It is well established that, when shock formation and propagation is analyzed within a continuum framework, the use of a viscous-dissipation term is mandatory for the attainment of a steady-wave shock profile. This fact has often been used as a justification for the use of a (local or global) thermostat within molecular-level simulations of shock-wave formation/propaga-
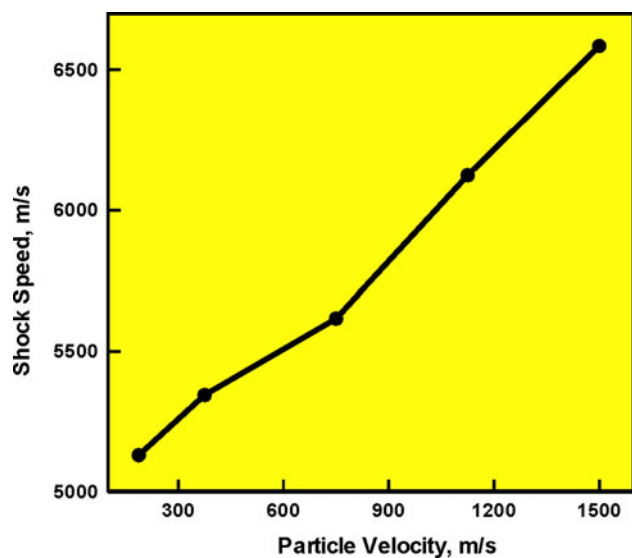
tion. While such practices greatly facilitate the attainment of a steady shock, they cannot be readily defended since shock formation and propagation is generally considered to be an adiabatic (no system/surrounding energy exchange) process due to the near-instantaneous material transition to the shocked state. In addition, shock generation/propagation is a non-isentropic process due to the attendance of various energy dissipation mechanisms. These were the determining factors in the decision to not use a thermostat in the present work. Due to the lack of a thermostat, the molecular dynamics simulations employed in the present work can be characterized as being of a non-equilibrium type. It is interesting to point out that despite the fact that no viscous-dissipation term was added to the Newton's equations of motion, the results displayed in Fig. 4(a)-(b) show some of the defining features of shock waves when they are analyzed in the continuum-level simulations (in the presence of viscous dissipation). Specifically, a steady shock is generated and the shock width decreases with an increase in the shock strength.

4.2 Determination of Shock Hugoniot Relations

The results presented in Fig. 4(a)-(b) reveal the steady-shock profile and can be used to find a functional relation between the shock speed, U_s, and the particle velocity, u_p. This was done in the present work and the results obtained are displayed in Fig. 5. The U_s vs. u_p relation is one of the so-called shock Hugoniot relations. In general, the Hugoniot can be defined as a locus of shocked-material states in a stress/pressure, energy density, mass density (or specific volume), temperature, particle velocity, and shock speed space which are associated with (or "centered at") a given initial/reference material state. The U_s vs. u_p relation mentioned above is a simple projection of the Hugoniot to the $U_s - u_p$ plane. In the case of planar shocks, of interest in the present work, the other commonly used Hugoniot relations include: axial stress, t_{11}, vs. density, ρ (or specific volume, $v = 1/\rho$); (mass-based) internal energy density, e, vs. ρ (or v); t_{11} vs. u_p and temperature T vs. ρ (or v). These relations were determined in the present work using two distinct methods:

(a) The first method is based on the three so-called "jump equations" which are defined as:

$$\rho^- U_\mathrm{s} = \rho^+ \left(U_\mathrm{s} - u_\mathrm{p} \right) \qquad \text{(Eq 6)}$$

$$t_{11}^- + \rho^- U_\mathrm{s}^2 = t_{11}^+ + \rho^+ \left(U_\mathrm{s} - u_\mathrm{p} \right)^2 \qquad \text{(Eq 7)}$$

$$e^- + \frac{t_{11}^-}{\rho^-} + 0.5 U_\mathrm{s}^2 = e^+ + \frac{t_{11}^+}{\rho^+} + 0.5 \left(U_\mathrm{s} - u_\mathrm{p} \right)^2 \qquad \text{(Eq 8)}$$

These equations relate the known downstream material states (denoted by a superscript "−") and the unknown upstream material states (denoted by a superscript "+") associated with the shock of a given strength (as quantified by the shock speed or the downstream-to-upstream particle velocity jump). These equations are next combined with the previously determined U_s vs. u_p relation and the prescribed (shock-strength defining quantity) U_s or u_p to solve for the unknown upstream material states. It should be noted that this method enables determination of only material mechanical state variables (t_{11}, e, v (=$1/\rho$), U_s, and u_p). To obtain temperature, a separate set of equilibrium NVE (E—total energy of the system) molecular dynamics simulations is carried out. In each case, a local computational sub-cell is defined containing only the upstream (shocked) material. The number of particles, the volume of the sub-cell and its total internal energy are all maintained constant. The associated "equilibrium" temperature is then calculated using the time-averages of the atomic velocities (see Eq 10); and

(b) Time averages of the atomic positions, r_i, velocities, v_i, and interaction forces, f_i (i is the atomic label) are used to compute the unknown, local (bin-based) thermo-mechanical quantities using the following standard statistical thermodynamic relations:

$$\rho = \frac{1}{V_\mathrm{bin}} \left[\left(\sum_{i=1}^{N_\mathrm{bin}} m_i \right)_\mathrm{avg} \right] \qquad \text{(Eq 9)}$$

$$T = \left(\frac{1}{3 N_\mathrm{bin} k_\mathrm{b}} \left[\sum_{i=1}^{N_\mathrm{bin}} m_i v_i . v_i \right] \right)_\mathrm{avg} \qquad \text{(Eq 10)}$$

$$t_{11} = \frac{1}{V_\mathrm{bin}} \left(N_\mathrm{bin} k_b T + \sum_{i=1}^{N_\mathrm{bin}} r_i \otimes f_i \right)_\mathrm{avg} \qquad \text{(Eq 11)}$$

$$E = \left(E_\mathrm{Total} + \frac{1}{2} \left(\sum_{i=1}^{N_\mathrm{bin}} m_i v_i \cdot v_i \right) \right)_\mathrm{avg} \qquad \text{(Eq 12)}$$

where subscript "avg" denotes time averaging, N_bin and V_bin the number of atoms within and the volume of the bin, respectively, k_b is the Boltzmann's constant, E_Total is given by Eq 1, while "·" and "$\otimes$" indicate dot product and tensorial product operators, respectively.

It should be noted that, in this case, the bins were defined within a reference frame which is attached to (and moves with) the steady-shock front. Clearly, in this case different atoms may reside within a given bin at different simulation times. On the other hand, the bins correctly collect the information about the atoms (temporarily) residing in a given segment of the steady-shock profile. In other words, time averages are calculated not for a fixed assembly of atoms, but rather for a transient set of atoms associated with a given moving bin. It should be also noted that since one of the main objectives of the present work was determination of the Hugoniot relations, only the data pertaining to the bins located in the fully shocked upstream region are collected and analyzed (for different shock-strength conditions). In other words, the data collected by the bins located within the shock profile and downstream of the shock are ignored.

The results of these two procedures are displayed in Fig. 6(a)-(d). In this figure, two cases are shown and labeled as "Method (a)" or "Method (b)" in order to indicate the method used for generation of the corresponding results. It is apparent that the two methods yield consistent results.

The Hugoniot relations displayed in Fig. 5 and 6(a)-(d) are typically used within a continuum-level computational analysis of shock-wave generation/ propagation in two ways:

(a) They are directly used in the analysis of shock-wave propagation under uniaxial strain conditions (Ref 30, 31); and

(b) Alternatively, they can be used to derive a continuum-level material model which is consistent with the material mechanical response under high-rate, large-strain, high-pressure conditions. Such a model is subsequently used in general three-dimensional, non-linear dynamics computational analyses (Ref 32).

In our recent work (Ref 6), it was shown that the Hugoniot relations can be generated by converting the corresponding isotherms (obtained via quasi-static, molecular-level mechanical tests). This procedure was found to be associated with a number of challenges (e.g., a particular form of the equation of state had to be assumed, several material properties/relations had to be assessed independently, etc.). Most of these challenges were not encountered in the present work since the Hugoniot relations are derived more directly from the molecular-level computational results.

4.3 Shock-Induced Material-State Changes

The results presented and discussed in the previous sections clearly revealed the formation and propagation of planar shocks in soda-lime glass and enabled formulation of the appropriate shock Hugoniot relations. In the present section, a more detailed investigation is carried out of the molecular-level material microstructure in the wake of a propagating planar shock.

It should be first realized that the analysis of material microstructure and its evolution due to shock loading in soda-lime glass is quite challenging due to the absence of a crystal structure in this material. Namely, when molecular-level simulations of shock generation/propagation are carried out in (nearly perfect) single crystal solids (Ref 17, 20), the presence of a crystal lattice greatly facilitates the investigation of deviations from the long range order (i.e., formation of various point, line and planar defects) and the nature of the associated inelastic deformation processes. Soda-lime glass is, on the other hand, an amorphous material in its initial condition and remains so after being subjected to shock loading. To address the challenge of material microstructure characterization and its changes resulting from shock loading, two microstructural parameters are monitored in the present work: (a) the extent of
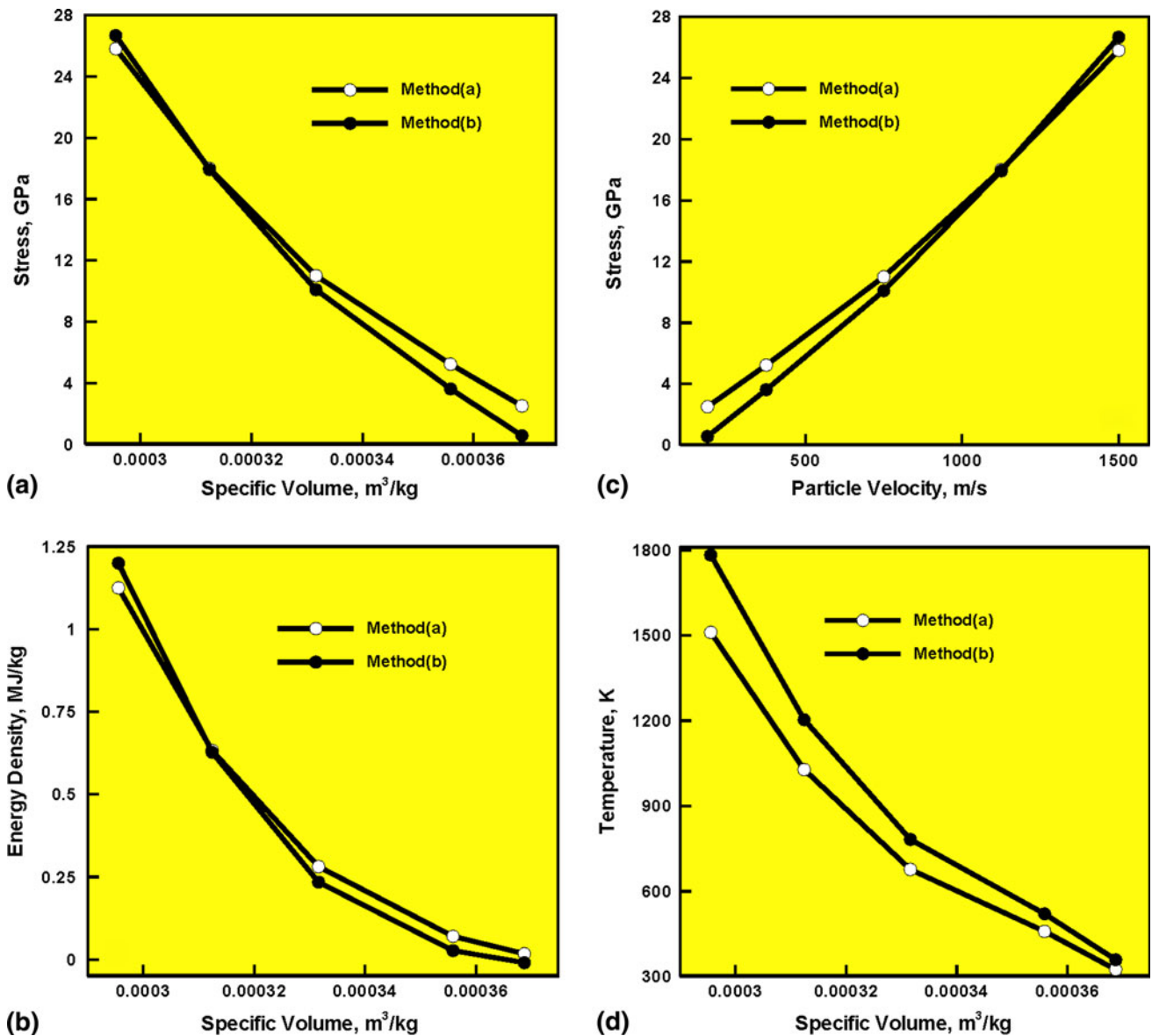
Fig. 6 (a) Axial stress vs. specific volume; (b) energy vs. specific volume; (c) axial stress vs. particle velocity; and (d) temperature vs. specific volume Hugoniot relations. Please see text for explanation of the "Method (a)" and "Method (b)"

lateral motion of the atoms at the shock front; and (b) the extent of changes to the Si and O atomic coordination (i.e., bonding structure).

In the case of single-crystalline solids, previous molecular-level shock-wave formation/calculation work (Ref 17, 20) established that the steady-wave condition is attained not as a result of (velocity-dependent) viscous dissipation (as is the case for shocks in fluids), but rather as a result of lateral atomic motions which result in inelastic deformation (permanent slippage of crystal planes and the formation of crystal defects). Similar lateral motions of the atoms at, or in the vicinity of, the shock front are also observed in the present work. Since these motions result in a permanent change in atomic nearest neighbor coordination (as well as in a permanent volume change of the shocked material), they can be considered as inelastic strain producing. However, as stated earlier, the amorphous nature of soda-lime glass precludes a more detailed/quantitative description of the nature of the atomic lateral

motion-induced inelastic-deformation process(s) or the associated microstructural defect formation. On the other hand, the accompanying changes in the atomic coordination and the bond structure can be readily identified (as will be demonstrated below).

Examples of the shock-loading induced changes in the atomic coordination and bond structure of soda-lime glass are given in Fig. 7(a)-(d) and 8(a)-(b). To aid in visualization/interpretation of the microstructural/topological changes experienced by soda-lime glass during shock loading, only a 20-30 atom exemplary region of the upstream material is analyzed in these figures. In addition, sodium cations are not displayed.

In Fig. 7(a) and (c), x-y and y-z projections are given of the material region under consideration in its initial state. The corresponding projections for the same material region after the passing of a shock are displayed in Fig. 7(b) and (d). A closer examination of the microstructure/topology results displayed in Fig. 7(a)-(d) provides clear evidence for the formation
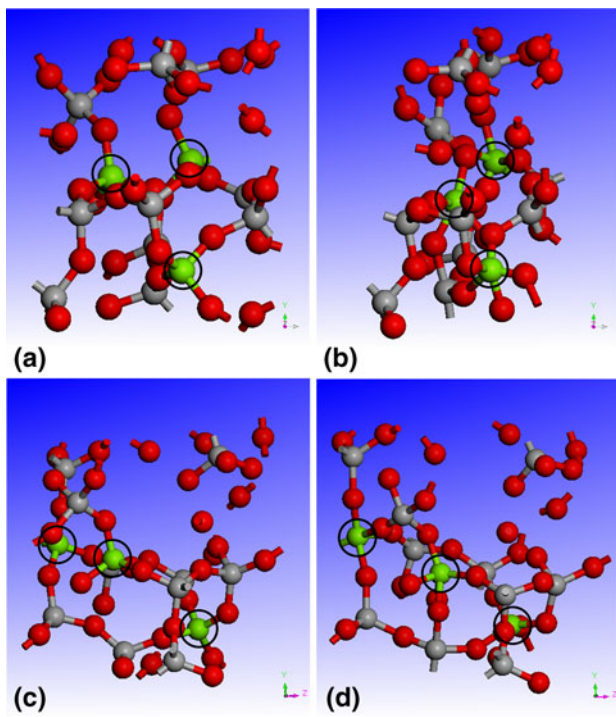
Fig. 7 Development of five-fold coordinated silicon atoms in soda-lime glass under shock loading: (a) material initial state, *x-y* projection; (b) post-shock state of the same material region as in (a); (c) and (d) correspond respectively to the *y-z* projection of (a) and (b)

of five-fold coordinated silicon atoms (circled for improved clarity). In addition, a comparison of the results displayed in Fig. 7(a)-(b) reveals the extent (partly irreversible) compaction caused by shock loading of soda-lime glass.

Additional typical changes in the soda-lime glass molecular-level microstructure induced by shock loading are displayed in Fig. 8(a)-(b). The results displayed in Fig. 8(a) pertain to the material initial state while those shown in Fig. 8(b) correspond to the shocked state of the same material region. A close examination of the results displayed in this figure reveals the formation of smaller Si-O rings. For improved clarity, these rings are highlighted in purple and yellow in Fig. 8(b).

It should be noted that the molecular-level microstructural changes described above are a manifestation of the transition of soda-lime glass to a state that is energetically favored at high shock-induced stresses (large densities). This finding is consistent with the experimental observation of Alexander et al. (Ref 32), who reported the formation of stishovite-like domains containing six-fold coordinated silicon atoms in soda-lime glass at ca. 30 GPa shock-induced axial stress levels.

It should be also recognized that shock loading leads to a permanent 2-4% (shock strength-dependent) increase in the material density. This material densification process along with the aforementioned processes leading to an increase in the silicon-atom coordination and smaller Si-O ring formation are all associated with energy absorption/dissipation and, hence, are expected to play an important role in the blast/ballistic impact mitigation potential of soda-lime glass.

4.4 Final Remarks

Within the present work, molecular-level computational methods are employed to study various phenomena accompa-
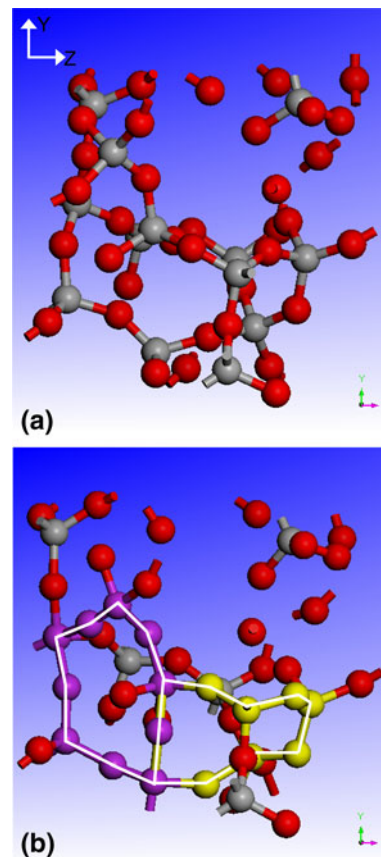

Fig. 8 Formation of smaller Si-O rings in soda-lime glass under shock loading: (a) material initial state, *y-z* projection; and (b) post-shock state of the same material region as in (a). Newly formed Si-O ring structures are highlighted for clarity

nying shock-wave generation and propagation in soda-lime glass. It should be noted that the present work does not suggest that molecular-level analyses of shock generation and propagation should replace the corresponding continuum-level (hydrodynamic) analyses. The latter are far better suited (and feasible) for studying the behavior of real-life engineering systems (e.g., vehicle windshield subjected to blast impact). Rather, the present approach is highly beneficial relative to the identification and characterization of the nanoscale phenomena/processes taking place at the shock front. Once these phenomena/processes are well understood and characterized (a formidable task) the knowledge gained can be used to formulate (and parameterize) more physically based material models suitable for use in continuum-level analyses.

5. Summary and Conclusions

Based on the results obtained in the present work, the following summary remarks and main conclusions can be drawn:

1. Various phenomena accompanying the formation and propagation of a planar shock wave within soda-lime glass, a material commonly used in transparent armor applications, are investigated using molecular-level computational methods.

2. The results obtained show that even without the use of a viscous-dissipation-based thermostat, a steady-wave planar shock profile can readily be established in this material.

3. The time-averaged results pertaining to the atomic positions, velocities and interaction forces are used to construct the appropriate shock Hugoniot relations, the relations which define the locus of stress, energy density, mass density, temperature and particle velocity in soda-lime glass swept by a shock propagating at a given speed.

4. Detailed examination of the molecular-level microstructure evolution in the shock-wave wake is carried out to identify the nature of energy-absorbing and shock wave spreading mechanisms. The results revealed that shock loading causes extensive changes in atomic coordination and the bond structure as well as a 2-4% (shock strength-dependent) density increase. Specifically, the atomic coordination of many silicon atoms has been found to increase from four to five and numerous smaller Si-O rings are observed. These processes are associated with substantial energy absorption and dissipation and are believed to greatly influence the blast/ballistic impact mitigation potential of soda-lime glass.

Acknowledgments

References

1. E. Strassburger, P. Patel, W. McCauley, and D.W. Templeton, Visualization of Wave Propagation and Impact Damage in a Polycrystalline Transparent Ceramic-AlON, *Proceedings of the 22nd International Symposium on Ballistics*, November 2005, Vancouver, Canada

2. AMPTIAC Quarterly, Army Materials Research: Transforming Land Combat Through New Technologies, *AMPTIAC Quart.*, 2004, **8**(4), p 2–5

3. M. Grujicic, B. Pandurangan, N. Coutris, B.A. Cheeseman, C. Fountzoulas, P. Patel, and E. Strassburger, A Ballistic Material Model for Starphire®, A Soda-lime Transparent Armor Glass, *Mater. Sci. Eng. A*, 2008, **492**(1), p 397–411

4. M. Grujicic, B. Pandurangan, W.C. Bell, N. Coutris, B.A. Cheeseman, C. Fountzoulas, and P. Patel, An Improved Mechanical Material Model for Ballistic Soda-Lime Glass, *J. Mater. Eng. Perform.*, 2009, **18**(8), p 1012–1028

5. M. Grujicic, B. Pandurangan, N. Coutris, B.A. Cheeseman, C. Fountzoulas, and P. Patel, A Simple Ballistic Material Model for Soda-Lime Glass, *Int. J. Impact Eng.*, 2009, **36**, p 386–401

6. M. Grujicic, W.C. Bell, P.S. Glomski, B. Pandurangan, B.A. Cheeseman, C. Fountzoulas, P. Patel, D.W. Templeton, and K.D. Bishnoi, Multi-length Scale Modeling of High-pressure Induced Phase Transformations in Soda-lime Glass, *J. Mater. Eng. Perform.*, 2010, **20**(7), p 1144–1156

7. L.V. Woodcock, C.A. Angell, and P. Cheeseman, Molecular Dynamics Studies of the Vitreous State: Simple Ionic Systems and Silica, *J. Chem. Phys.*, 1976, **65**, p 1565–1577

8. R.G.D. Valle and E. Venuti, High-Pressure Densification of Silica Glass: A Molecular-dynamics Simulation, *Phys. Rev. B*, 1996, **54**(6), p 3809–3816

9. K. Trachenko and M.T. Dove, Densification of Silica Glass Under Pressure, *J. Phys.: Condens. Matter*, 2002, **14**, p 7449–7459

10. Y. Liang, C.R. Miranda, and S. Scandolo, Mechanical Strength and Coordinate Defects in Compressed Silica Glass: Molecular Dynamics Simulations, *Phys. Rev. B*, 2007, **75**, p 024205

11. B. Nghiem, PhD thesis, University of Paris 6, France 1998

12. C. Denoual and F. Hild, Dynamic Fragmentation of Brittle Solids: A Multi-scale Model, *Eur. J. Mech. Solids A*, 2002, **21**, p 105–120

13. M. Yazdchi, S. Valliappan, and W. Zhang, A Continuum Model for Dynamic Damage Evolution of Anisotropic Brittle Materials, *Int. J. Numer. Methods Eng.*, 1996, **39**, p 1555–1583

14. F. Hild, C. Denoual, P. Forquin, and X. Brajer, On the Probabilistic and Deterministic Transition Involved in a Fragmentation Process of Brittle Materials, *Comput. Struct.*, 2003, **81**, p 1241–1253

15. T.J. Holmquist, D.W. Templeton, and K.D. Bishnoi, Constitutive Modeling of Aluminum Nitride for Large Strain High-strain Rate, and High-pressure Applications, *Int. J. Impact Eng.*, 2001, **25**, p 211–231

16. G.T. Camacho and M. Ortiz, Computational Modeling of Impact Damage in Brittle Materials, *Int. J. Solids Struct.*, 1996, **33**, p 20–22, 2899–2938

17. B.L. Holian and G.K. Straub, Molecular Dynamics of Shock Waves in Three-Dimensional Solids: Transition from Nonsteady to Steady Waves in Perfect Crystals and Implications for the Rankine-Hugoniot Conditions, *Phys. Rev. Lett.*, 1979, **43**, p 1598

18. G.K. Straub, S.K. Schiferl, and D.C. Wallace, Thermodynamic Properties of Fluid Sodium from Molecular Dynamics, *Phys. Rev. B*, 1983, **28**, p 312–316

19. V. Y. Klimenko and A. N. Dremin, in *Detonatsiya, Chernogolovka*, O. N. Breusov et al., Eds., AkademiiNauk, Moscow, 1978, p 79

20. B.L. Holian, W.G. Hoover, B. Moran, and G.K. Straub, Shock-Wave Structure Via Non-equilibrium Molecular Dynamics and Navier-Stokes Continuum Mechanics, *Phys. Rev. A*, 1980, **22**, p 2498

21. W.D. Kingery, H.K. Bowen, and D.R. Uhlmann, *Introduction to Ceramics*, 2nd ed., John Wiley & Sons, New York, 1976, p 91–124

22. H. Sun, COMPASS: An ab Initio Force-Field Optimized for Condensed-Phase Applications Overview with Details on Alkane and Benzene Compounds, *J. Phys. Chem. B*, 1998, **102**, p 7338–7364

23. H. Sun, P. Ren, and J.R. Fried, The COMPASS force field: parameterization and validation for phosphazenes, *Comput. Theoret. Polym. Sci.*, 1998, **8**(1/2), p 229–246

24. http://www.accelrys.com/mstudio/msmodeling/visualiser.html

25. http://www.accelrys.com/mstudio/msmodeling/amorphouscell.html

26. M. Grujicic, Y.P. Sun, and K.L. Koudela, The Effect of Covalent Functionalization of Carbon Nanotube Reinforcements on the Atomic-level Mechanical Properties of Poly-Vinyl-Ester-Epoxy, *Appl. Surf. Sci.*, 2007, **253**, p 3009

27. http://www.accelrys.com/mstudio/msmodeling/discover.html

28. D.N. Theodorou and U.W. Suter, Atomistic Modeling of Mechanical Properties of Polymeric Glasses, *Macromolecules*, 1986, **19**, p 139–154

29. A.V. Amirkhizi, J. Isaacs, J. McGee, and S. Namet-Nasser, An Experimentally-Based Viscoelastic Constitutive Model for Polyurea, Including Pressure and Temperature Effects, *Philos. Mag.*, 2006, **86**(36), p 5847–5866

30. M. Grujicic, W.C. Bell, B. Pandurangan, and T. He, Blast-Wave Impact Mitigation of Polyurea When Used as a Helmet Suspension-Pad Material, *Mater. Des.*, 2010, **31**(9), p 4050–4065

31. M. Grujicic, W. C. Bell, B. Pandurangan and P. S. Glomski, Fluid/Structure Interaction Computational Investigation of the Blast-wave Mitigation Efficiency of the Advanced Combat Helmet, *J. Mater. Eng. Perform.*, in press, 2010

32. C.S. Alexander, L.C. Chhabildas, W.D. Reinhart, and D.W. Templeton, Changes to the Shock Response of Fused Quartz Due to Glass Modification, *Int. J. Impact Eng.*, 2008, **35**, p 1376–1385